Scanning Tunneling Spectroscopic Studies of the Low-Energy Quasiparticle Excitations in Cuprate Superconductors

N.-C. Yeh, M. L. Teague, R. T.-P. Wu, Z. J. Feng, H. Chu, A. M. Moehle

Department of Physics, California Institute of Technology, Pasadena, CA 91125

1-626-395 4313

1-626-395 3955

ncyeh@caltech.edu

http://www.its.caltech.edu/~yehgroup

Original paper for the Proceedings of ICSM2012, Istanbul (April 29 – May 4)

We report scanning tunneling spectroscopic (STS) studies of the low-energy quasiparticle excitations of cuprate superconductors as a function of magnetic field and doping level. Our studies suggest that the origin of the pseudogap (PG) is associated with competing orders (COs), and that the occurrence (absence) of PG above the superconducting (SC) transition T_c is associated with a CO energy Δ_{CO} larger (smaller) than the SC gap Δ_{SC}. Moreover, the spatial homogeneity of Δ_{SC} and Δ_{CO} depends on the type of disorder in different cuprates: For optimally and under-doped $YBa_2Cu_3O_{7-\delta}$ (Y-123), we find that $\Delta_{SC} < \Delta_{CO}$ and that both Δ_{SC} and Δ_{CO} exhibit long-range spatial homogeneity, in contrast to the highly inhomogeneous STS in $Bi_2Sr_2CaCu_2O_{8+x}$ (Bi-2212). We attribute this contrast to the stoichiometric cations and ordered apical oxygen in Y-123, which differs from the non-stoichiometric Bi-to-Sr ratio in Bi-2212 with disordered Sr and apical oxygen in the SrO planes. For Ca-doped Y-123, the substitution of Y by Ca contributes to excess holes and disorder in the CuO_2 planes, giving rise to increasing inhomogeneity, decreasing Δ_{SC} and Δ_{CO}, and a suppressed vortex-solid phase. For electron-type cuprate $Sr_{0.9}La_{0.1}CuO_2$ (La-112), the homogeneous Δ_{SC} and Δ_{CO} distributions may be attributed to stoichiometric cations and the absence of apical oxygen, with $\Delta_{CO} < \Delta_{SC}$ revealed only inside the vortex cores. Finally, the vortex core radius (ξ_{halo}) in electron-type cuprates is comparable to the SC coherence length ξ_{SC}, whereas $\xi_{halo} \sim 10\xi_{SC}$ in hole-type cuprates, suggesting that ξ_{halo} may be correlated with the CO strength. The vortex-state irreversibility line in the magnetic field versus temperature phase diagram also reveals doping dependence, indicating the relevance of competing orders to vortex pinning.

Keywards: cuprate superconductivity; pseudogap; competing orders; quasiparticle excitations; scanning tunneling spectroscopy

Abbreviations: SC; PG; COs; STS; LDOS; FT-LDOS; Y-123; Bi-2212, La-112

1. Introduction

The low-energy quasiparticle excitations of cuprate superconductors exhibit various spectral characteristics that differ from those of simple Bogoliubov quasiparticles for pure superconductors because of the presence of competing orders (COs) in the ground state of under- and optimally doped cuprates [1-10]. Some of the best known unconventional spectral characteristics include: the presence (absence) of pseudogap and Fermi arc phenomena in hole-type (electron-type) cuprates [4-12]; dichotomy of the quasiparticle coherence for momentum near the nodal and anti-nodal parts of the Fermi surface [9,12,13]; pseudogap (PG)-like spectral features inside vortex cores [4-7]; and non-universal spectral homogeneity among different types of cuprates [4,5,14-18].

In this work we investigate the effects of varying doping levels and magnetic fields on the spatially resolved low-energy quasiparticle excitations of hole- and electron-type cuprate superconductors. Our experimental results suggest that the PG phenomena are closely related to COs, and that the correlation of superconductivity (SC) and PG with different types of disorder may account for the varying degrees of spatial homogeneity in the quasiparticle spectra. We also demonstrate the effect of hole doping on the vortex-state irreversibility line, which suggests the relevance of competing orders to vortex pinning.

2. Experimental

The primary experimental technique employed in this work is cryogenic scanning tunneling spectroscopy (STS). Details of the experimental setup, surface preparations and methodology of data analysis for the STS studies have been described elsewhere [5-7,14,15]. The hole-type cuprates investigated in this work include optimally and under-doped Y-123 single crystals with SC transition temperatures T_c = 93 K, 85 K and 60 K, which correspond to hole doping levels of p = 0.15, 0.13 and 0.09, respectively; and over-doped $(Y_{1-x}Ca_x)Ba_2Cu_3O_{7-\delta}$ epitaxial films grown by pulsed laser deposition with x = 0.05, 0.10, 0.125, 0.20 and 0.30, and the corresponding T_c determined from magnetization measurements were 68 K, 64 K, 59 K, 42 K and 74 K, respectively. We note that the p value for a given Ca-doping level x depends on the oxygen annealing process [19], and that there is a maximum T_c value for a given x, $T_{c,max}(x)$, which were empirically

determined to be 93.5 K, 89.0 K, 82.9 K and 82.9 K for $x = 0$, 0.10, 0.20 and 0.30, respectively [19]. Hence, the p values of Ca-doped Y-123 samples are estimated from $T_{c,max}(x)$ and the empirical formula [20] $T_c(x,p) = T_{c,max}(x)$ $[1–82.6(p–0.16)^2]$, yielding p = 0.216, 0.218, 0.214, 0.238 and 0.19 for x = 0.05, 0.10, 0.125, 0.20 and 0.30. The electron-type cuprate studied in this work is an optimally doped infinite-layer system $Sr_{0.9}La_{0.1}CuO_2$ (La-112) with T_c = 43 K [7,15]. All samples had been characterized by x-ray diffraction and magnetization studies to ensure single-phased structures and superconductivity. In addition to microscopic STS studies, the effects of Ca-doping on macroscopic vortex dynamics were investigated by measuring the irreversibility temperature $T_{irr}(H,x,p)$ from the zero-field-cool (ZFC) and field-cool (FC) magnetization (M) vs. temperature (T) curves [21].

3. Doping Dependent Quasiparticle Tunneling Spectra and Vortex Dynamics

Spatially resolved tunneling conductance (dI/dV) vs. energy ($\omega = eV$) spectra for the quasiparticle local density of states (LDOS) maps at T = 6 K were obtained on aforementioned Y-123, Ca-doped Y-123, and La-112 samples in zero and finite magnetic fields (H). For H = 0, the tunneling spectra revealed long-range spatial homogeneity in under- and optimally doped Y-123 and optimally doped La-112 samples [4-7], which differ from the strong spatially inhomogeneous tunneling spectra observed in Bi-2212 [17,18]. In contrast, for Ca-doped Y-123, the zero-field LDOS spectra revealed spatial homogeneity only within a limited range (up to $\sim 10^2$ nm in length); variations in the spectral characteristics appeared over a long range, which may be attributed to disorder in Ca-doping.

3.1 Doping dependent zero-field LDOS of hole-type cuprates

A representative zero-field LDOS of the optimally doped Y-123 in the top panel of Fig. 1a shows a set of coherent peaks at $\omega = \pm\Delta_{SC}$ and shoulder-like features at $\pm\Delta_{eff}$. Both features exhibit long-range spatial homogeneity, as manifested by the histogram in the bottom panel of Fig. 1a. We attribute the two features to the consequence of coexisting SC and CO in the ground state of the under- and optimally doped hole-type cuprates [4-10]. Briefly, the LDOS $\mathcal{N}(\omega)$ is associated

with the spectral density function $A(\mathbf{k},\omega)$ and the Green function $G(\mathbf{k},\omega)$ by the relation $\mathcal{N}(\omega) = \sum_{\mathbf{k}} A(\mathbf{k},\omega) = -\sum_{\mathbf{k}} \mathrm{Im}[G(\mathbf{k},\omega)]/\pi$, and $G(\mathbf{k},\omega)$ may be obtained from diagonalizing the mean-field Hamiltonian $\mathcal{H}_{\mathrm{MF}} = \mathcal{H}_{\mathrm{SC}} + \mathcal{H}_{\mathrm{CO}}$ that consists of coexisting SC and a CO, where $\mathcal{H}_{\mathrm{SC}}$ is given by [4-10]

$$\mathcal{H}_{\mathrm{SC}} = \sum_{\mathbf{k},\alpha} \xi_{\mathbf{k}} c^{\dagger}_{\mathbf{k},\alpha} c_{\mathbf{k},\alpha} - \sum_{\mathbf{k}} \Delta_{\mathrm{SC}}(\mathbf{k}) \left(c^{\dagger}_{\mathbf{k},\uparrow} c^{\dagger}_{-\mathbf{k},\downarrow} + c_{-\mathbf{k},\downarrow} c_{\mathbf{k},\uparrow} \right).$$

Here the SC pairing potential is given by $\Delta_{\mathrm{SC}}(\mathbf{k}) = \Delta_{\mathrm{d}}(\cos k_x - \cos k_y)/2$ for pure $d_{x^2-y^2}$-wave pairing and $\Delta_{\mathrm{SC}}(\mathbf{k}) = \Delta_{\mathrm{d}}(\cos k_x - \cos k_y)/2 + \Delta_{\mathrm{s}}$ for ($d_{x^2-y^2}$+s)-wave pairing [14], $\mathbf{k}$ denotes the quasiparticle momentum, $\xi_{\mathbf{k}}$ is the normal-state eigen-energy relative to the Fermi energy, $c^{\dagger}$ and c are the creation and annihilation operators, and $\alpha = \uparrow, \downarrow$ refer to the spin states. For $\mathcal{H}_{\mathrm{CO}}$, there is a CO energy Δ_{CO} and a density wave-vector associated with a given CO [4-10]. In the case of charge density waves (CDW) being the relevant CO, we have a $\mathbf{Q}_1$ parallel to the CuO_2 bonding direction $(\pi,0)/(0,\pi)$ [4-10]. The LDOS thus obtained for the optimally doped Y-123 is shown by the solid line in Fig. 1a, where $\Delta_{\mathrm{eff}} \equiv [(\Delta_{\mathrm{d}})^2 + (\Delta_{\mathrm{CO}})^2]^{1/2}$. We further note the occasional occurrence of a zero-bias conductance peak (ZBCP) for tunneling along the {100} direction, as exemplified in the main panel of Fig. 1a, which is the result of the atomically rugged {100} surface so that Andreev bound states near {110} can contribute to the tunneling spectra, as detailed in Ref. [14].

For under-doped Y-123, the zero-field LDOS also reveals similar spectral features (Fig. 1b, upper panel), except that Δ_{d} is reduced and Δ_{eff} evolves from shoulder-like features to peak-like features separated from the SC coherence peaks. Both Δ_{d} and Δ_{eff} remain spatially homogeneous (Fig. 1b, lower panel).

In the case of Ca-doped Y-123, the pairing symmetry evolves from pure $d_{x^2-y^2}$ to ($d_{x^2-y^2}$+s)-wave with $\Delta_{\mathrm{SC}}(\mathbf{k}) = \Delta_{\mathrm{d}}(\cos k_x - \cos k_y)/2 + \Delta_{\mathrm{s}}$ [14,22,23], and the spectral characteristics are homogeneous only over smaller areas $\sim(10^2 \times 10^2)$ nm^2 probably due to disordered Ca-doping. As exemplified in Fig. 1c for a Ca-doped Y-123 with $x = 0.3$ and $p \sim 0.19$, two sets of coherent peaks appear at $\omega = \pm(\Delta_{\mathrm{d}}+\Delta_{\mathrm{s}})$ and $\pm(\Delta_{\mathrm{d}}-\Delta_{\mathrm{s}})$ [14], and the shoulder-like features correspond to $\Delta_{\mathrm{eff}} = [(\Delta_{\mathrm{SC}})^2 + (\Delta_{\mathrm{CO}})^2]^{1/2}$, where $\Delta_{\mathrm{SC}} \equiv \max\{\Delta_{\mathrm{SC}}(\mathbf{k})\}$. The doping dependent Δ_{SC} and Δ_{CO}

for the Y-123 system is shown in Fig. 1d, showing a dome-like $\Delta_{SC}(p)$ similar to that of $T_c(p)$ and a decreasing $\Delta_{CO}(p)$ similar to the PG temperature $T^*(p)$.

3.2 Vortex-state LDOS of hole-type cuprates

In the vortex state of conventional type-II superconductors, SC inside the vortex core is suppressed by the supercurrents surrounding each vortex, giving rise to enhanced local density of states (LDOS) peaking at $\omega = 0$ near the center of each vortex [24]. In contrast, the vortex-state LDOS of Y-123 exhibits several important differences. First, despite spatially homogeneous zero-field LDOS, field-induced vortices are relatively disordered and the radius of the vortex "halo" ($\xi_{halo} \sim 10$ nm) appears much larger than the SC coherence length $\xi_{SC} \sim 1.2$ nm, (Fig. 2a). Further, the vortex-state LDOS remains suppressed inside the vortex core (Figs. 2c-2d), with PG-like features appearing at the same energy Δ_{CO} as that derived from theoretical analysis of the zero-field LDOS. Moreover, density-wave like constant-bias conductance modulations are apparent, as exemplified in Fig. 2b. The histogram of the spectral evolution from Δ_{SC} to Δ_{CO} and another sub-gap feature at Δ' with increasing H is shown in Fig. 2e, which is in stark contrast to the vortex-state spectral evolution of conventional type-II superconductors [4].

To obtain further insights, we perform Fourier transformation (FT) of the LDOS at constant energies (ω). As shown in Fig. 3a for the FT-LDOS in the reciprocal space for spectra integrated from −1 to −30 meV, various spectral peaks are apparent, which may be divided into two distinct types: One is associated with the ω-independent wave-vectors that may be attributed to COs of charge-, pair- and spin-density waves (CDW, PDW and SDW) and the (π,π) magnetic resonance, as shown in Figs. 3b, 3d and summarized in Fig. 3g [4-6]. The other type consists of ω-dependent quasiparticle interference (QPI) wave-vectors [5,6,17], as exemplified in Fig. 3e and summarized in Fig. 3f. The spectral intensity of these ω-independent wave-vectors exhibits interesting evolution with H that further corroborates the existence of COs, as exemplified in Fig. 3c [4-6].

3.3 LDOS of electron-type cuprates

The zero-field LDOS of electron-type cuprate La-112 exhibited a single set of spectral peaks at $\omega = \pm\Delta_{eff}$ (Fig. 4a), and the LDOS revealed long-range spatial

homogeneity [7]. Theoretical fitting to the LDOS and the k-dependent spectral density from angle-resolved photoemission spectroscopy (ARPES) yields a $d_{x^2-y^2}$-wave SC gap with $\Delta_d \sim 12$ meV and a SDW with a wave-vector of (π,π) and $\Delta_{SDW} \sim 8$ meV [4,5,7]. The vortex-state LDOS of La-112 revealed a vortex-core radius comparable to $\xi_{SC} \sim 4.9$ nm. The LDOS remained suppressed inside the vortex core, with PG-like features appearing at $\Delta_{CO} < \Delta_{SC}$, as shown in Fig. 4c. The fact that $\Delta_{CO} < \Delta_{SC}$ is consistent with the absence of zero-field PG above T_c in La-112. The histogram of the spectral evolution with H is illustrated in Fig. 4d, which differs from those of Y-123 (Fig. 2e) and conventional type-II superconductors.

3.4 Doping dependent vortex dynamics

In addition to the LDOS, we investigate how vortex dynamics may evolve with different doping. By applying H parallel to the CuO_2 planes of Y-123 and Ca-doped Y-123 and determining the irreversibility temperatures $T_{irr}(H,p,x)$ from the ZFC and FC M-vs.-T curves [21], we find that the normalized irreversibility line that separates the vortex-solid from the vortex-liquid initially decreases with increasing Ca-doping x for nearly constant p (Fig. 5), suggesting suppressed SC coherence due to Ca-induced disorder [23]. As the hole doping further increases, the trend eventually reverses (Fig. 5), probably due to vanishing COs and therefore enhanced SC stiffness and reduced vortex-state fluctuations [21].

4. Discussion

In addition to the doping dependence of Δ_{SC} and Δ_{eff}, it is interesting to address the issue of spatial homogeneity of LDOS in different cuprates. Comparing our empirical findings with the highly inhomogeneous quasiparticle spectra in Bi-2212 [17,18], it appears that the spatial homogeneity in the LDOS depends on the type of disorder: For optimally and under-doped Y-123, the long-range spatial homogeneity in both Δ_{SC} and Δ_{eff} may be attributed to the stoichiometric cations and ordered apical oxygen. In contrast, for Ca-doped Y-123, the substitution of Y by Ca contributes to excess holes as well as disorder in the CuO_2 planes, giving rise to spatial variations in Δ_{SC} and Δ_{eff}. In the case of under and optimally doped Bi-2212, the non-stoichiometric Bi-to-Sr ratio results in disordered Sr and apical oxygen in the SrO layer [25], leading to highly disordered PG features. Finally,

for optimally doped electron-type cuprate La-112, the homogeneous LDOS may be attributed to stoichiometric cations and the absence of apical oxygen.

5. Conclusion

Scanning tunneling spectroscopic studies of various cuprate superconductors as a function of doping level, doping type and magnetic field (H) reveal that their low-energy excitations consist of not only the Bogoliubov quasiparticles but also bosonic excitations associated with COs, leading to a PG above T_c for $H = 0$ and inside the vortex core for $T << T_c$ if $\Delta_{CO} > \Delta_{SC}$, as in the under- and optimally doped Y-123. In contrast, for $\Delta_{CO} < \Delta_{SC}$ as in the electron-type cuprate La-112 and strongly over-doped Y-123, PG is absence above T_c for $H = 0$ and is only revealed inside the vortex core for $T << T_c$. The vortex core size ξ_{halo} for cuprates with $\Delta_{CO} > \Delta_{SC}$ is much larger than ξ_{SC}, whereas ξ_{halo} for cuprates with $\Delta_{CO} < \Delta_{SC}$ is comparable to ξ_{SC}, suggesting that the vortex core states are sensitive to the CO strength. The microscopic doping-dependent spectral characteristics are found to be relevant to the macroscopic vortex dynamics, as manifested by the doping dependent vortex irreversibility lines of Y-123.

We acknowledge funding provided by NSF Grant #DMR0907251, by the Institute for Quantum Information and Matter, an NSF Physics Frontiers Center with support of the Gordon and Betty Moore Foundation, and by the Kavli Nanoscience Institute with support of the Kavli Foundation. ZJF acknowledges the support from China Scholarship Council during his visit to Caltech.

References

1. Sachdev, S.: Rev. Mod. Phys. **75**, 913 (2003)
2. Kivelson, S.A., et al.: Rev. Mod. Phys. **75**, 1201 (2003)
3. Demler, E., Hanke, W. Zhang, S.-C.: Rev. Mod. Phys. **76**, 909 (2004)
4. Yeh, N.-C., Beyer, A.D.: Int. J. Mod. Phys. B **23**, 4543 (2009)
5. Yeh, N.-C., et al.: J. Supercond. Nov. Magn. **23**, 757 (2010)
6. Beyer, A.D., et al.: Europhys. Lett. **87**, 37005 (2009)
7. Teague, M.L., et al.: Europhys. Lett. **85**, 17004 (2009)
8. Yu, B.-L., et al.: Solid State Commun. **149**, 261 (2009)
9. Chen, C.-T., Beyer, A.D., Yeh, N.-C.: Solid State Commun. **143**, 447 (2007)
10. Beyer, A.D., Chen, C.-T., Yeh, N.-C.: Physica C **468**, 471 (2008)
11. Fischer, O., et al.: Rev. Mod. Phys. **79**, 353 (2007)
12. Damascelli, A., Hussain, Z., Shen, Z.-X.: Rev. Mod. Phys. **75**, 473 (2003)

13. Zhou, X.J., et al.: Phys. Rev. Lett. **92**, 187001 (2004).
14. Yeh, N.-C., et al.: Phys. Rev. Lett. **87**, 087003 (2001)
15. Chen, C.-T., et al.: Phys. Rev. Lett. **88**, 227002 (2002)
16. Bobroff, J., et al.: Phys. Rev. Lett. **89**, 157002 (2002)
17. McElroy, K., et al.: Phys. Rev. Lett. **94**, 197005 (2005)
18. McElroy, K., et al.: Science **309**, 1048 (2005)
19. Fisher, B., et al.: Phys. Rev. B **47**, 6054 (1993)
20. Presland, M.R., et al.: Physica C **176**, 95 (1991)
21. Beyer, A.D., et al.: Phys. Rev. B **76**, 140506(R) (2007)
22. Limonov, M.F., Rykov, A.I., Tajima, S.: Phys. Rev. B **61**, 12412 (2000)
23. Uykur, E., et al.: Phys. Rev. B **84**, 184527 (2011)
24. Hess, H., et al.: Phys. Rev. Lett. **64**, 2711 (1990)
25. Zhou, S., Ding, H., Wang, Z.: Phys. Rev. Lett. **98**, 076401 (2007)

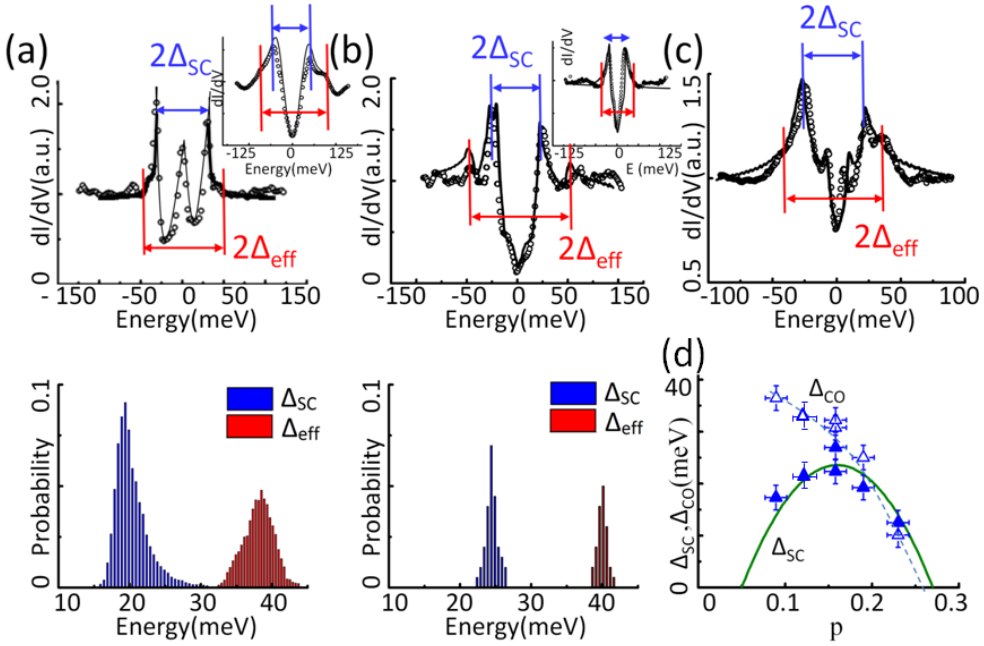

Fig. 1: (Color online) Doping dependent zero-field STS in Y-123 taken at T = 6 K: **(a)** Upper panel: Normalized LDOS of optimally doped Y-123 (T_c = 93 K) with k || {100} and {001} (inset). The solid lines represent theoretical fittings [4-10] by assuming coexisting SC and CDW with parameters Δ_{SC} = 29 (21) meV for k || {100} ({001}), Δ_{CDW} = 32 meV and Q_{CDW} = (0.25π ± 0.05π,0)/(0,0.25π ± 0.05π), and the zero-bias conductance peak in the main panel is due to atomically rugged {100} surface so that some of the Andreev bound states near {110} are detected and fit with the BTK theory [14]. Lower panel: Histograms for Δ_{SC} and Δ_{CDW}. **(b)** Upper panel: Normalized LDOS of under-doped Y-123 (T_c = 60 K) with k || {100} and {001} (inset, T_c = 85 K). Lower panel: Histograms for Δ_{SC} and Δ_{CDW}. **(c)** Normalized LDOS of Ca-doped Y-123 with k || {001}, T_c = 74 K and p = 0.19. The parameters are (Δ_d, Δ_s, Δ_{CDW}) = (16, 3, 27) meV. **(d)** Zero-field Δ_{SC} and Δ_{CDW} of Y-123 *vs.* p.

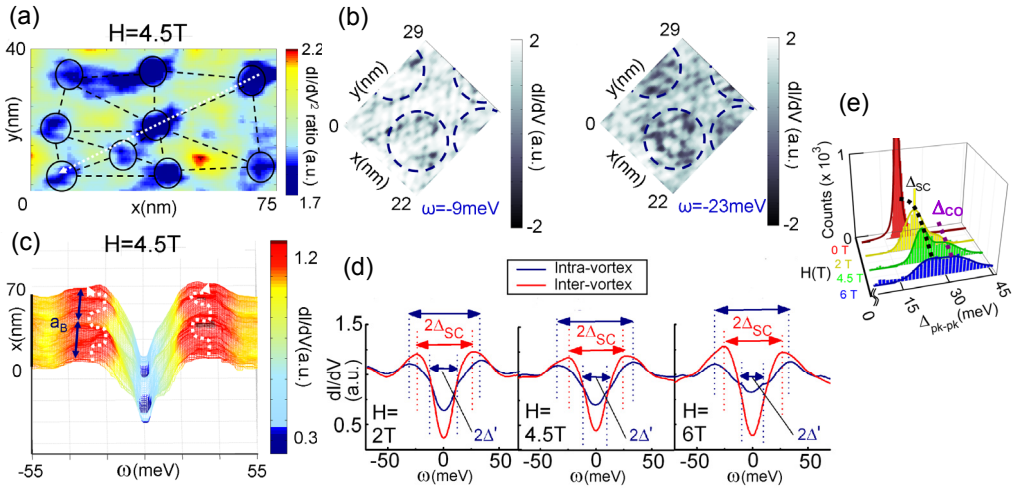

Fig. 2: (Color online) Spatially resolved STS studies of the vortex-state of Y-123 at $T = 6$ K [5,6]: **(a)** Tunneling conductance power ratio r_G map over a (75×40) nm^2 area for $H = 4.5$ T, showing a_B = (23.5±8.0) nm. Here r_G at each pixel is defined by the ratio of $(dI/dV)^2$ at $V = (\Delta_{SC}/e)$ to that at $V = 0$. **(b)** The LDOS modulations of Y-123 at $H = 5$ T over a (22×29) nm^2 area, showing patterns associated with density-wave modulations and vortices (circled objects) for $\omega = -9$ meV $\sim -\Delta'$ and $\omega = -23$ meV $\sim -\Delta_{SC}$. **(c)** Conductance spectra along the white line in (a), showing SC peaks at $\omega = \pm\Delta_{SC}$ outside vortices and PG features at $\omega = \pm\Delta_{CO}$ inside vortices. **(d)** Spatially averaged intra- and intervortex spectra for $H = 2.0$ T, 4.5 T and 6 T from left to right. **(e)** Energy histograms for the field-dependent spectral weight derived from the STS data for $H = 0$, 2, 4.5, and 6T, showing a spectral shift from Δ_{SC} to Δ_{CO} and Δ' with increasing H.

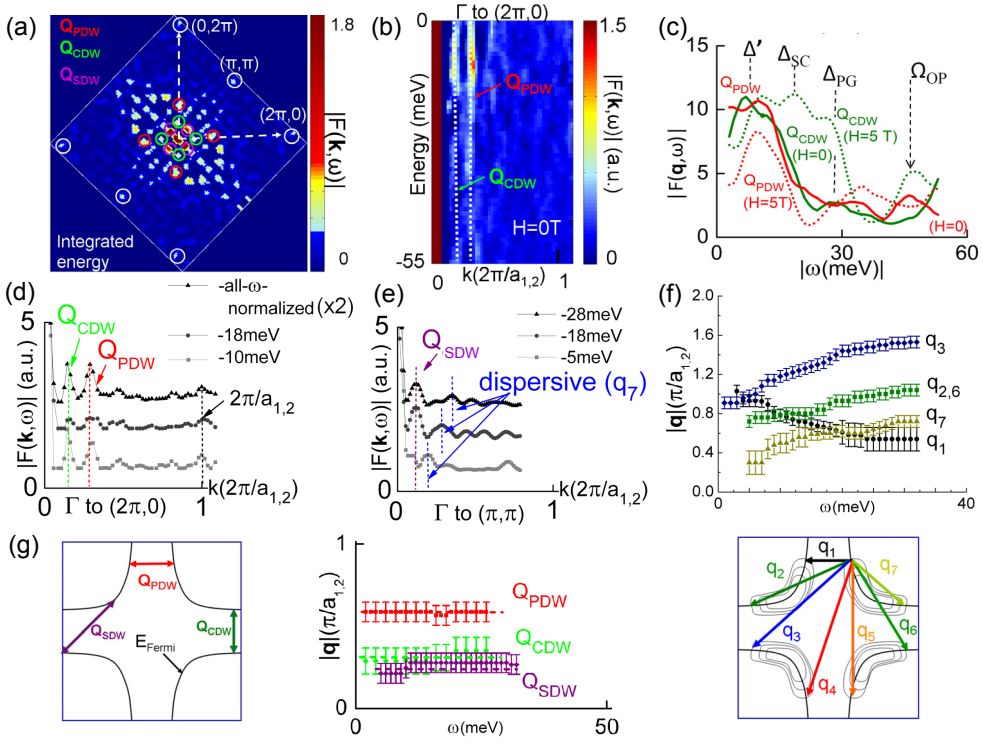

Fig. 3: (Color online) Studies of the vortex-state FT-LDOS of Y-123 [4-6]: **(a)** FT-LDOS at $H = 5$ T obtained by integrating $|F(\mathbf{k},\omega)|$ from $\omega = -1$ meV to -30 meV. The ω-independent spots are circled for clarity, which include the reciprocal lattice constants, the (π,π) resonance, $\mathbf{Q}_{PDW}$ and $\mathbf{Q}_{CDW}$ along the $(\pi,0)/(0,\pi)$ directions, and $\mathbf{Q}_{SDW}$ along (π,π). **(b)** The ω-dependence of $|F(\mathbf{k},\omega)|$ at $H = 5$ T is plotted in the ω-*vs.*-$\mathbf{k}$ plot against $\mathbf{k} \parallel (\pi,0)$, showing ω-independent modes (bright vertical lines) at $\mathbf{Q}_{PDW}$ and $\mathbf{Q}_{CDW}$. **(c)** $|F(\mathbf{q},\omega)|$ for $\mathbf{q} = \mathbf{Q}_{PDW}$ (red) and $\mathbf{Q}_{CDW}$ (green) are shown as a function of ω for $H = 0$ (solid lines) and $H = 5$ T (dashed lines). **(d)** $|F(\mathbf{k},\omega)|$ for different energies are plotted against $\mathbf{k} \parallel (\pi,0)$, showing peaks at ω-independent Q_{PDW}, Q_{CDW} and the reciprocal lattice constants at $(2\pi/a_1)$ along $(\pi,0)$. **(e)** $|F(\mathbf{k},\omega)|$ for different energies are plotted against $\mathbf{k} \parallel (\pi,\pi)$, showing peaks at ω-independent Q_{SDW} along (π,π). Additionally, dispersive wave vectors due to QPI are found, as exemplified by the dispersive QPI momentum $\mathbf{q}_7$ specified in Fig. 3(f). **(f)** The QPI momentum ($|\mathbf{q}_i|$) vs. ω dispersion relations derived from FT-LDOS [4-6]. Lower panel: Illustration of the $\mathbf{q}_i$ associated with QPI between pairs of points on equal energy contours with maximum joint density of states. **(g)** Left panel: Illustration of the wave-vectors associated with SDW and CDW. Right panel: ω-independent $|\mathbf{Q}_{PDW}|$, $|\mathbf{Q}_{CDW}|$ and $|\mathbf{Q}_{SDW}|$ [4-6].

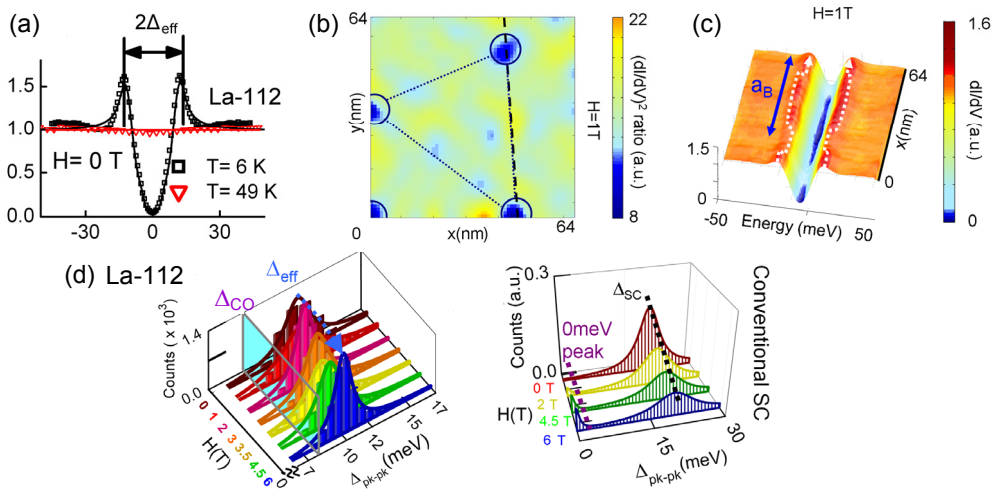

Fig. 4: (Color online) STS studies of La-112: **(a)** Normalized tunneling spectra taken at T = 6 K (black) and 49 K (red) for H = 0. The solid lines represent fittings to the T = 6 and 49 K spectra by assuming coexisting SC and SDW, with fitting parameters Δ_d = 12 meV, $\Delta_{CO} = \Delta_{SDW}$ = 8 meV, and $Q_{SDW} = (\pi,\pi)$ [4,5,7]. **(b)** A spatial map of the r_G ratio over a (64×64) nm^2 area for H (||c) = 1 T and T = 6 K, showing vortices separated by an average vortex lattice constant a_B = 52nm, comparable to the theoretical value of 49 nm. The average radius of vortices is ξ_{halo} = (4.7±0.7) nm, comparable to ξ_{SC} = 4.9 nm. **(c)** Spatial evolution of (dI/dV) along the black dashed line cutting through two vortices in (b) for H = 1T, showing an intra-vortex PG smaller than the inter-vortex SC gap. **(d)** Energy histograms of La-112 (left), which differ from those of conventional type-II SC (right).

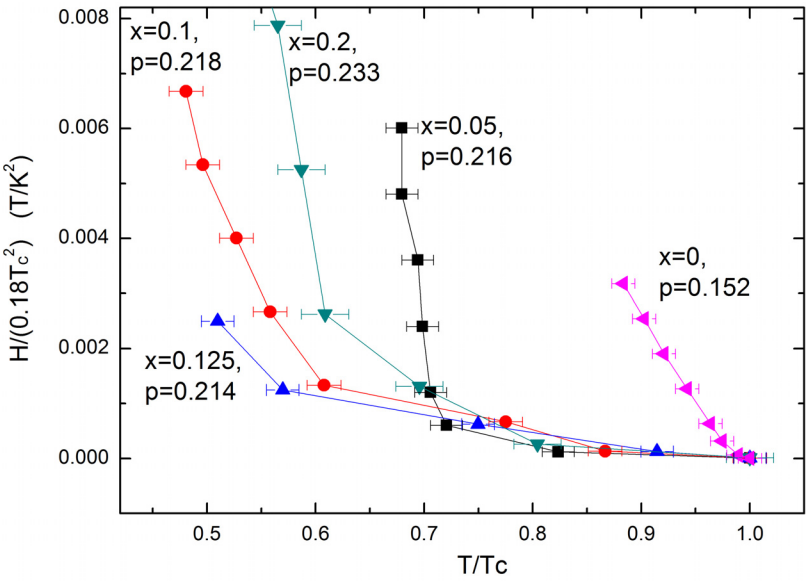

Fig. 5: Vortex irreversibility lines vs. (T/T_c) for $H \parallel ab$ in Y-123 systems, where the irreversibility field $H_{irr}(T,x,p)$ for each sample is normalized to its respective theoretical upper critical field $[H_{c2}(0)]_{ab}$ by the relation $[H_{c2}(0)]_{ab} = \Phi_0/[2\pi\xi_{ab}(0)\xi_c(0)]$. Using the mean-field gap relation $2\Delta_d = 4.3k_BT_c$ for *d*-wave pairing and the BCS relation $\Delta_d = hv_F/[2\pi\xi_{ab}(0)]$, where h is the Plank constant and v_F is the Fermi velocity (~10^5 m/s in the cuprates), we obtain $[H_{c2}(0)]_{ab} \sim (0.18\ \text{Tesla/K}^2)\times(T_c)^2$ for T_c measured in K by using the empirical anisotropy ratio $\gamma = \xi_{ab}(0)/\xi_c(0) \sim 7$ [21]. For $x < 0.2$, the vortex solid phase below the normalized irreversibility line $H_{irr}(T,x,p)/(0.18T_c^2)$ is suppressed with increasing Ca-doping if p is kept nearly constant. However, for sufficiently large hole-doping levels (such as for $p > 0.23$), the trend is reversed due to vanishing CO and increasing SC stiffness.